Title
Protein aggregation in salt solutions

Journal
Proceedings of the National Academy of Sciences of the United States of America, 112(21)

ISSN
0027-8424

Authors
Kastelic, Miha
Kalyuzhnyi, Yurij V
Hribar-Lee, Barbara
et al.

Publication Date
2015-05-26

DOI
10.1073/pnas.1507303112

Peer reviewed

Protein aggregation in salt solutions

Miha Kastelic[a], Yurij V. Kalyuzhnyi[b], Barbara Hribar-Lee[a], Ken A. Dill[c,1], and Vojko Vlachy[a]

[a]Faculty of Chemistry and Chemical Technology, University of Ljubljana, 1000 Ljubljana, Slovenia; [b]Institute for Condensed Matter Physics, 79011 Lviv, Ukraine; and [c]Laufer Center for Physical and Quantitative Biology and Departments of Physics and Chemistry, Stony Brook University, Stony Brook, NY 11794

Contributed by Ken A. Dill, April 20, 2015 (sent for review January 16, 2015; reviewed by Shekhar Garde and John M. Prausnitz)

Protein aggregation is broadly important in diseases and in formulations of biological drugs. Here, we develop a theoretical model for reversible protein–protein aggregation in salt solutions. We treat proteins as hard spheres having square-well-energy binding sites, using Wertheim's thermodynamic perturbation theory. The necessary condition required for such modeling to be realistic is that proteins in solution during the experiment remain in their compact form. Within this limitation our model gives accurate liquid–liquid coexistence curves for lysozyme and γ IIIa-crystallin solutions in respective buffers. It provides good fits to the cloud-point curves of lysozyme in buffer–salt mixtures as a function of the type and concentration of salt. It than predicts full coexistence curves, osmotic compressibilities, and second virial coefficients under such conditions. This treatment may also be relevant to protein crystallization.

phase separation | protein aggregation | Hofmeister series

Protein molecules can aggregate with each other. This process is important in many ways (1). First, a key step in developing biotech drugs—which are mostly mABs—is to formulate proteins so that they do not aggregate. This is because good shelf-life requires long-term solution stability, and because patient compliance requires liquids having low viscosities. The importance of such formulations comes from the fact that the world market for protein biologicals is about the same size as for smartphones. Second, protein aggregation in the cell plays a key role in protein condensation diseases, such as Alzheimer's, Parkinson's, Huntington's, and others. Third, much of structural biology derives from the 100,000 protein structures in the Protein Data Bank, a resource that would not have been possible without protein crystals, a particular state of protein aggregation. Also, it is not yet possible to rationally design the conditions for proteins to crystallize.

However, protein aggregation is poorly understood. Atomistic-level molecular simulations are not practical for studying multiprotein interactions as a function of concentration, and in liquid solutions that are themselves fairly complicated—that account for salts of different types and concentrations as well as other ligands, excipients, stabilizers, or metabolites. So, a traditional approach is to adapt colloid theories, such as the Derjaguin–Landau–Verwey–Overbeek (DLVO) (2) theory. In those treatments, proteins are represented as spheres that interact through spherically symmetric van der Waals and electrostatic interactions in salt water, using a continuum representation of solvent and a Debye–Hückel screening for salts. DLVO often gives correct trends for the pH and salt concentration dependencies. However, DLVO does not readily account for protein sequence-structure properties, salt bridges (which are commonly the "glue" holding protein crystals together), explicit waters in general, or Hofmeister effects, where different salts have widely different powers of protein precipitation (3–5). A more subtle treatment is required for these effects (6–8).

Coarse-grained statistical mechanics is essential for describing the properties of complex solutions. For proteins, such modeling needs to go beyond central-force approximations because it is generally noted that "the isotropic models fail to describe the phase diagram of protein solutions quantitatively and cannot address phenomena such as protein aggregation and self-assembly" (9, 10), typically yielding coexistence curves that are too narrow and/or overestimating the critical temperature of the phase diagram. Accounting for the discreteness of protein charges (11, 12) leads to better predictions, for example of small-angle neutron scattering (13). Another approach for treating the potential asymmetries is to assume heterogeneously charged surfaces, in the so-called patchy models (9, 14–17). Recent results for the gas–liquid and fluid–solid coexistence equilibria for this type of model are in good agreement with experiments on lysozyme solutions, but it requires the assumption of a temperature-dependent pseudo-potential (16). However, another approach is to assume the range and directionality of attractive interactions varies around the protein (9, 12, 18). A key conclusion from these works is that to properly capture protein liquid-phase equilibria seems to require that the range of interactions between proteins be short (18–22).

Modeling proteins as rigid bodies has severe limitations, as pointed out in the recent paper of Sarangapani et al. (23) and highlighted by Prausnitz (24). When analyzing protein aggregation by such models, these studies indicate the importance of knowing that during the experiment the native structure is preserved. It is recommended to use CD as a tool for verifying that no changes in protein conformation take place during experiments.

The cloud-point temperature measurements modeled here were described in refs. 25 and 26. In experiments the temperature was first decreased until the transmitted beam would disappear and then raised until the original scattering intensity was restored. Reversible opacification was indicative that protein remained in the compact state. The transition between the single-phase and the two-phase region is reversible and without hysteresis also for other proteins (see ref. 1, p. 165). Further evidence on stability of the lysozyme, which is the central molecule of our analysis, is provided in ref. 27, figure 6. The CD

Significance

Protein aggregation is a problem in amyloid and other diseases, and it is a challenge when formulating solutions of biological drugs, such as monoclonal antibodies. The physical processes of aggregation, especially in salt solutions, are not well understood. We model a protein as having multiple binding sites to other proteins, leading to orientational variations, dependent on salt. With few parameters and with knowledge of the cloud-point temperatures as a function of added salt, the model gives good predictions for properties including the liquid–liquid coexistence curves, the second virial coefficients, and others for lysozyme and gamma-crystallin.

Author contributions: B.H.-L. and V.V. designed research; M.K. and Y.V.K. performed research; Y.V.K. helped create software; V.V. supervised the research; and K.A.D. and V.V. wrote the paper.

Reviewers: S.G., Rensselaer Polytechnic Institute; and J.M.P., University of California, Berkeley.

The authors declare no conflict of interest.

[1]To whom correspondence should be addressed. Email: dill@laufercenter.org.

This article contains supporting information online at www.pnas.org/lookup/suppl/doi:10.1073/pnas.1507303112/-/DCSupplemental.

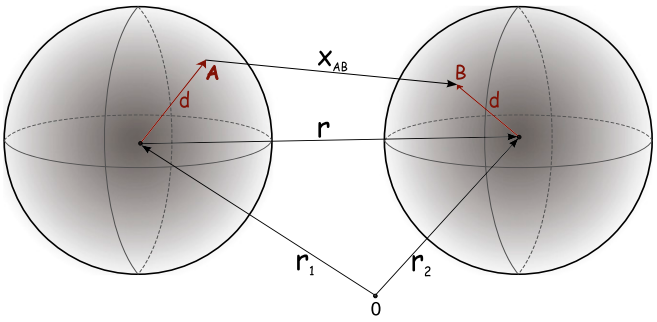

Fig. 1. Proteins interact as two spheres. They interact at $M \times M$ pairs of binding sites on the surfaces, one pair of which (A and B) is indicated here.

spectra of the lysozyme remain unchanged during the solubility studies performed at protein concentrations similar to (or even higher than) those modeled here.

The perturbed hard-sphere models, similar to the one proposed below, have been successfully used before (see, e.g., refs. 19, 22, 25, 28, and 29). In these and other similar models the perturbation part of potential was assumed to be isotropic. In contrast to this we treat the protein–protein interaction as directional. We model proteins as hard spheres, with a number of square-well attractive sites located on the surface, which we call the "binding sites." In this aspect our approach resembles some simple water models (30, 31). The modification seems to have significant consequences for the shape of the liquid–liquid coexistence curve. We treat the solution physics through the thermodynamic perturbation theory that was developed by Wertheim for liquids that are strongly associating (32, 33). The model is used to analyze various experimental data.

Methods

We model the protein solution as a one-component system of N protein molecules with number density $\rho = N/V$ at temperature T and volume V. The protein molecules are represented as spheres of diameter σ embedded in the solvent composed of water, buffer, and various simple salts. The solvent is simply treated as an effective modifier of the protein–protein interactions.

We assume that the protein–protein pair potential is composed of (*i*) the hard-sphere part $u_R(r)$ and (*ii*) attractive contributions, u_{AB}, caused by the (short-range) square-well sites localized on the surface of the protein (32):

$$u(\boldsymbol{r}) = u_R(r) + \sum_{A\epsilon\Gamma}\sum_{B\epsilon\Gamma} u_{AB}(\boldsymbol{x}_{AB}). \quad [1]$$

Here, $\boldsymbol{r}$ ($r = |\boldsymbol{r}|$) is the vector between the centers of molecules, $\boldsymbol{x}_{AB}$ is the vector connecting sites A and B on two different molecules, and Γ denotes the set of sites (Fig. 1). We examine a special case, where M sites are randomly distributed over the surface of the spherical protein. Note that $d = 0.5\sigma$. The identical binding potential u_{AB} acts among all sites. The pairwise additive potential is then written as

Table 1. Model parameters used in the lysozyme and γ IIIa–crystallin calculations

Parameter	Lysozyme	γ IIIa-crystallin
σ, nm	3.43	3.78
M_2, g·mol^{-1}	14,300	20,700
M	10	14
ϵ_W/k_B, K	2,360	2,490
a_W, nm	0.18	0.18

M_2 is the molar mass of the protein.

$$u_R(r) = \begin{cases} \infty & \text{for } r < \sigma, \\ 0 & \text{for } r \geq \sigma, \end{cases} \quad [2]$$

$$u_{AB}(\boldsymbol{x}_{AB}) = \begin{cases} -\varepsilon_W & \text{for } |\boldsymbol{x}_{AB}| < a_W, \\ 0 & \text{for } |\boldsymbol{x}_{AB}| \geq a_W. \end{cases} \quad [3]$$

Here ε_W (>0) is the square-well depth of the binding potential and a_W is its range. The interaction acts only when the site–site distance $|\boldsymbol{x}_{AB}|$ is smaller than a_W, the square-well width. We avoid nonphysical multisite bonding by applying the following restriction (32, 34):

$$0 < a_W < \sigma - \sqrt{3}d. \quad [4]$$

Next, we assume that the free energy A of the solution is additive:

$$A = A^{id} + A^{hs} + A^{ass}, \quad [5]$$

where A^{id} is the ideal free energy, A^{hs} is the hard sphere, and A^{ass} the site–site association contribution to the free energy. This latter term is adopted from Wertheim's thermodynamic perturbation theory (32, 33, 35):

$$\frac{\beta A^{ass}}{N} = M\left(\ln X - \frac{X}{2} + \frac{1}{2}\right), \quad [6]$$

where $\beta = (k_B T)^{-1}$ and k_B is Boltzmann's constant. The association parameter X defines the average fraction of molecules not bonded to any site and is determined by the mass-action law (35):

$$X = \frac{1}{1 + MX\rho\Delta_{AB}}. \quad [7]$$

The term Δ_{AB} is defined by the expression (34)

$$\Delta_{AB} = 4\pi g^{hs}(\sigma) \int_{\sigma}^{2d+a_W} \bar{f}_{ass}(r) r^2 dr, \quad [8]$$

where $\bar{f}_{ass}(r)$ is the angular average of the Mayer function, obtained as described in ref. 34 (see also Eqs. S9 and S10). The radial distribution function $g^{hs}(r)$ is obtained from the analytical solution of the Ornstein–Zernike integral equation within the Percus–Yevick (PY) approximation (36).

Once the free energy A of the solution is known, we compute the pressure P (effectively, the osmotic pressure) and chemical potential μ of the proteins using the standard equations (36):

$$\mu = \left[\frac{\partial(A/V)}{\partial\rho}\right]_{T,V}, \quad [9]$$

$$P = \rho\mu - \frac{A}{V}. \quad [10]$$

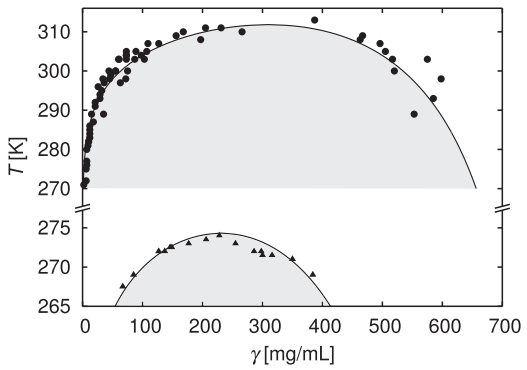

Fig. 2. Liquid–liquid phase separation, two-phase region is indicated by shaded area: lysozyme (▲) (pH 6.0, phosphate buffer of ionic strength 0.6 mol·dm^{-3}) (25) and γ IIIa-crystallin (•) (pH 7.1, phosphate buffer, 0.24 mol·dm^{-3}) (26) solutions. Solid curves are calculated from our model, based on the parameters in Table 1. The critical temperatures above which we have one-phase regions are estimated to be 274 ± 2 K for lysozyme and 312 ± 2 K for γ IIIa-crystallin.

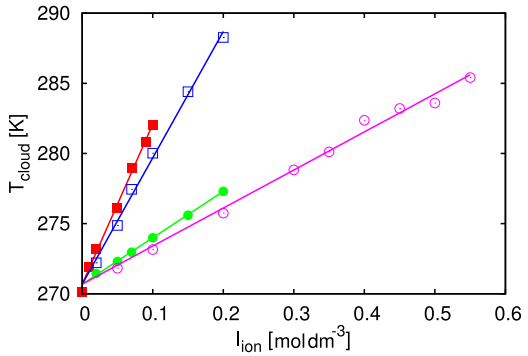

Fig. 3. T_{cloud} for lysozyme as a function of ionic strength of the added alkali-halide salts I_{ion}: symbols denote experimental data (pH 6.8, $I_{tot} = 0.6$ mol·dm^{-3}, phosphate buffer and added alkali-halide salts) (25) and the lines are results of Eq. **12**. The parameters are from Table 2. From top to bottom: KBr (filled red square), NaBr (open blue square), KCl (filled green circle), and NaCl (open pink circle) salts.

These quantities are critical for the calculation later of the coexistence curve. An additional quantity of practical interest is the second virial coefficient B_2, which is defined through the relation

$$\beta P = \rho + B_2\rho^2 + \ldots. \quad [11]$$

It is useful (37) to give this quantity as a dimensionless parameter $B_2^* = B_2/B_2^{(hs)}$, where $B_2^{(hs)}$ is the hard-sphere contribution to the second virial coefficient, equal to $2\pi\sigma^3/3$ (36). Another interesting measurable quantity, obtained by scattering techniques, is the osmotic compressibility $\chi_{osm} = \beta(\partial P/\partial\rho)_{N,T}$. For more details of the actual computation see *Supporting Information*.

Numerical Results and Comparison with Experimental Data

Besides the diameter of the protein σ, parameters of the model are the number M of attractive square-well sites and the depth ϵ_W and range a_W of the square-well potential. We obtain them as follows. First, we choose the number of attractive sites M; numerical studies indicate that the critical density on the coexistence curve depends mainly on this quantity (14). Two other parameters that influence the shape of coexistence curves are the square-well depth ϵ_W and its range a_W. ϵ_W affects the critical temperature, and a_W determines the breadth of the coexistence curve. Notice that the range of the potential is restricted by Eq. **4** to be smaller than $0.134\,\sigma$. We fix $a_W = 0.18$ nm to be equal to the length of a hydrogen bond (38). Finally, we set ϵ_W to get the correct critical temperature. We find best fits of $\epsilon_W = 19.6$ kJ/mol for lysozyme and 20.7 kJ/mol for γ IIIa-crystallin (see also Table 1). Both values are in the range of the hydrogen-bond strengths (38) and are consistent with experiments on hydrogen bonds and salt bridges across protein–protein interfaces (4).

Liquid–Liquid Coexistence Curves and Cloud-Point Temperatures. Many liquid–liquid phase separation curves have been published (e.g., refs. 25, 26, 39, and 40)—more than we can reference here. In Fig. 2 we fit our calculations to the experimental liquid–liquid phase diagrams of lysozyme and γ IIIa-crystallin published in refs. 25 and 26. In these graphs γ is the mass concentration of protein, equal to $\rho M_2/N_A$, where N_A is Avogadro's number. The best-fit parameters are given in Table 1. The maximum peak-point temperature on such curves is the critical temperature above which there is no two-phase region.

Protein aggregation has also been studied as a function of the types and concentrations of added salt in the surrounding solution. What is commonly studied is the cloud-point temperature, T_{cloud} (25, 40). This is the temperature at which the cloudiness in the solution signals the onset of protein aggregation. In important work, Taratuta et al. (25) determined cloud-point temperatures for lysozyme–phosphate buffer mixtures. At buffer ionic strengths ranging from 0.3 to 0.6 mol·dm^{-3} (at pH 6.8), Taratuta et al. (25) found no change in the cloud-point temperature. This can be attributed to the strong electrostatic screening of the protein–protein charge interactions at high buffer concentration.

Taratuta et al. (25) also studied the effects of added alkali-halide salts (NaCl, KCl, NaBr, and KBr) to the solution, at the same time decreasing the buffer content to keep the total ionic strength, I_{tot}, fixed at 0.6 mol·dm^{-3}. In other words, the electrolyte present in addition to the protein contains $I_{tot} - I_{ion}$ of buffer and I_{ion} of alkali-halide salt. Fig. 3 shows that T_{cloud} is linearly proportional to the ionic strength of added alkali-halide salt I_{ion}. Slopes of these curves are determined by the salt type (39, 40). An increase of T_{cloud} can be interpreted as an increased attraction between protein molecules at increased alkali-halide salt ionic strength I_{ion}. Considering that total ionic strength I_{tot} is constant (but not the ionic composition, because part of the buffer content is replaced by another salt), this effect can be ascribed to specific-salt effects occurring at the protein surface. This assumption is supported by the observation of distinctly different slopes for different anions. Notice that lysozyme at

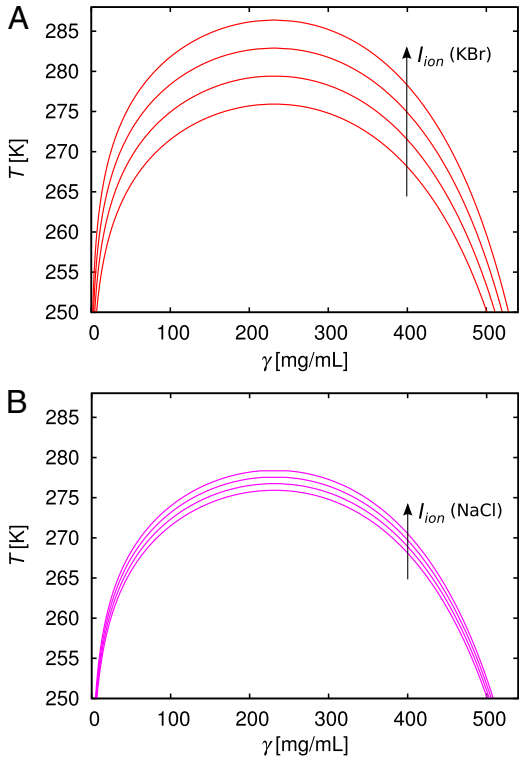

Fig. 4. The calculated coexistence curves for lysozyme in the buffer–salt mixtures. Calculations are based on Eq. **12** and parameters from Table 2. (*A*) KBr and (*B*) NaCl are added to the buffer keeping the total ionic strength $I_{tot} = 0.6$ mol·dm^{-3} constant. Increase of I_{ion} (bottom to top) from 0 to 0.09 mol·dm^{-3} in steps of 0.03 mol·dm^{-3} (pH 6.8) causes an increase in the critical temperature.

Table 2. Parameters *a* (K·dm^3·mol^{-1}) and *b* = 2,374 (K) defining Eq. 12

Parameter	KBr	KCl	NaBr	NaCl
a	1,000	290	790	238

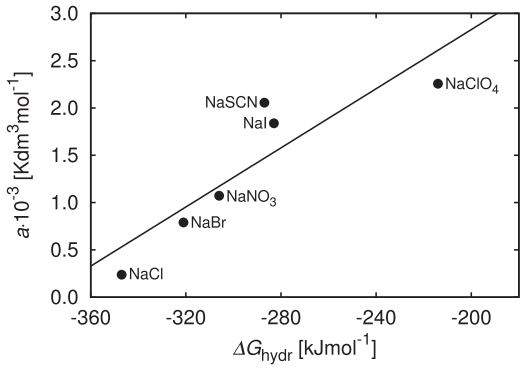

Fig. 5. Specific ion effects in lysozyme solutions: correlation of the slope a of Eq. **12** with the hydration Gibbs free energies ΔG_{hydr} (43) of the corresponding anions. The line is the best least-square fit through the data.

pH 6.8 has a positive net charge; this explains why the effect of anions in Fig. 3 is stronger than that of cations.

Within our model, we capture salt effects simply by supposing the well depth is proportional to the ionic strength, I_{ion}, of the added alkali-halide salt:

$$\epsilon_W(I_{ion})/k_B = a \cdot I_{ion} + b. \quad [12]$$

The best-fit slopes and intercept parameters for the different salts are given in Table 2. Notice that for $I_{ion} = 0$ we recover pure buffer–lysozyme (no alkali-halide salts present) mixture, with cloud-point temperature around 271 K, and $\epsilon_W/k_B = b$. In Fig. 2 we show the liquid–liquid phase diagram of lysozyme for the case where $I_{tot} = 0.6$ mol·dm^{-3} and $I_{ion} = 0$ (measurements were not made for $I_{ion} > 0$). One practical application of our model is in leveraging experimental cloud-point data from Fig. 3 for predicting complete liquid–liquid phase diagrams; see Fig. 4. This figure shows the prediction that in the range of $I_{ion} \in [0,0.09]$, the critical temperature for protein aggregation is increased much more by adding KBr than by adding NaCl salt. No experiments are yet available to test these full phase-diagram predictions.

How can we rationalize the effects of added alkali-halide salts at constant ionic strength on cloud points? First, why should the well depth increase with ionic strength of added alkali-halide salts? The effect seems to be due to the adsorption of (halide) ions to the protein–solution surface. Zhang and Cremer (40) showed that specific-salt dependence of T_{cloud} can be modeled by a modified Langmuir binding isotherm. Under conditions where the concentration of adsorbing ions in the mixture is low, the adsorption should be proportional to the I_{ion} of the added salt. This explains experimental results for T_{cloud} shown in Fig. 3. In our simple model, the linearity between T_{cloud} and I_{ion} translates into the linear dependence of ϵ_W on I_{ion} (see Eq. **12**).

Second, can we rationalize the different effects of different types of salts? Fig. 5 gives some insight. It shows that ions that are most strongly solvated by water (which are the ions having the smallest radii, for atomic ions) are those that have the smallest effect (the smallest slopes a) on cloud-point temperatures. The ions that most readily release hydration waters most strongly affect the protein–protein attraction. In Fig. 5, we correlate the slopes a in Eq. **12**, fitting experimental data, with the hydration Gibbs free energies ΔG_{hydr} of anions for sodium salts. To analyze the effects of addition of NaBr, NaCl, $NaNO_3$, NaI, NaSCN, and $NaClO_4$ to lysozyme solutions in water we combine the measurements from two sources (25, 40). The ordering of salts follows the so-called inverse Hofmeister series (40). The findings above are in line with our recent polyelectrolyte studies (41, 42).

Second Virial Coefficient and Osmotic Compressibility. The second virial coefficient is a principal measure of pairwise protein–protein interactions in solution. In recent years, the second virial coefficient has become an important tool for understanding and predicting protein crystallization conditions (28, 29, 44–52). George and Wilson (44) were the first to notice that the conditions that best promote protein crystallization are those that fall within a particular "crystallization slot" of values of the second virial coefficient, B_{22}. The favorable range of B_{22} values for which proteins should crystalize from a water–salt mixture is between -2×10^{-4} and -8×10^{-4} cm^3·mol·g^{-2} (44, 49). B_{22} is calculated on the basis of the protein mass concentration γ and is related to B_2 in Eq. **11** as $B_{22} = B_2 N_A / M_2^2$.

Rarely are experimental measurements made on a given type of protein of all of the properties of aggregation together—the cloud point, the liquid–liquid phase coexistence curves, the second virial coefficient, and/or the osmotic compressibility. Systematic experiments could give deep insights into aggregation. However, this is a virtue of the present model: From a single type of experiment, such as cloud-point measurements, we can compute all of the rest. For example, Fig. 6 shows our calculated B_2 curves for lysozyme in buffer–salt mixtures under experimental conditions of Fig. 3. For lysozyme the crystallization slot is approximately between $B_2^* = -0.8$ and -3.2. This means that bromide salts would fall in this range at lower I_{ion} than chloride salts at this pH. We are not aware of experimental data for testing this prediction.

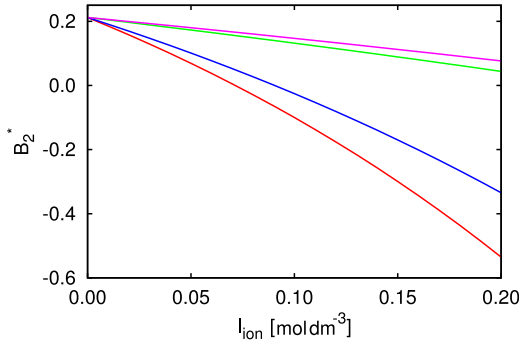

Fig. 6. Calculated B_2^* for lysozyme buffer – salt mixtures at $T = 300$ K: experimental conditions (pH 6.8, $I_{tot} = 0.6$ mol·dm^{-3}) (25); see Fig. 3. From bottom to top: KBr, NaBr, KCl, and NaCl additions (calculations based on Eq. **12** and parameters from Table 2) to buffer.

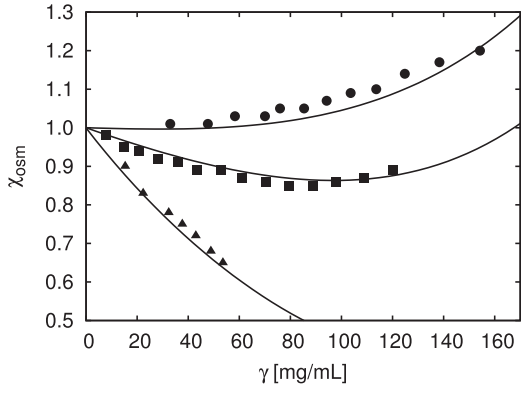

Fig. 7. Osmotic compressibility χ_{osm} for lysozyme–NaCl mixtures at pH 4.6 (symbols denote experimental data from ref. 28) and theoretical predictions (lines) for different NaCl concentrations: 0.15 (●), 0.25 (■), and 0.45 (▲) mol·dm^{-3}. We changed the scale of the x axis from ρ (28) to γ concentration units.

SYSTEMS BIOLOGY

The osmotic compressibility $\chi_{osm} = \beta(\partial P/\partial \rho)_{N,T}$ data can be obtained by scattering techniques (see, e.g., refs. 28 and 53). Rosenbaum et al. (28) determined χ_{osm} of lysozyme in acetate buffer–salt mixtures at pH 4.6. Fig. 7 shows our calculations of osmotic compressibilities, with ϵ_W/k_B calculated from Eq. **12** (lines), compared with the experimental data on lysozyme–NaCl mixtures (28) (symbols). Good fits of experimental results are obtained for $a = 760$ K·mol^{-1}·dm^3 and $b = 2{,}628$ K, with $M = 6$ at this protein charge at this pH.

Conclusions

We have developed here a largely analytical model for protein–protein aggregation equilibria in salt solutions. Proteins are modeled as hard spheres having M binding sites that interact with a square-well depth and width in the range of the hydrogen-bond values. Unlike simpler models, the binding sites lead to orientational interactions between the proteins. With those few parameters and with knowledge of the cloud-point temperatures as a function of salt concentration, we compute the range of experimentally measurable aggregation properties—such as the liquid–liquid coexistence curves, the second virial coefficients, and the osmotic compressibilities. Where data are currently available, the model captures them well. We believe this model may be useful for developing protein formulations and for deeper understanding of the driving forces of protein aggregation.

ACKNOWLEDGMENTS. We thank Prof. J. M. Prausnitz for fruitful discussions on limitations of colloidal models and Profs. G. B. Benedek and A. Lomakin for helpful correspondence regarding experimental data. This study was supported by the Slovenian Research Agency fund through Program 0103–0201, by NIH Grant GM063592, and the Young Researchers Program (M.K.) of the Republic of Slovenia.

1. Gunton JD, Shiryayev A, Pagan DL (2007) *Protein Condensation: Kinetic Pathways to Crystallization and Disease* (Cambridge Univ Press, Cambridge, UK).
2. Verwey EJ, Overbeek JTG (1948) *Theory of the Stability of Lyophobic Colloids* (Elsevier, Amsterdam).
3. Collins KD (1997) Charge density-dependent strength of hydration and biological structure. *Biophys J* 72(1):65–76.
4. Xu D, Tsai CJ, Nussinov R (1997) Hydrogen bonds and salt bridges across protein-protein interfaces. *Protein Eng* 10(9):999–1012.
5. Kunz W, ed (2009) *Specific Ion Effects* (World Scientific, Teaneck, NJ).
6. Lima ERA, Biscaia EC, Boström M, Tavares FW, Prausnitz JM (2007) Osmotic second virial coefficients and phase diagrams for aqueous proteins from a much-improved Poisson-Boltzmann equation. *J Chem Phys C* 111(43):16055–16059.
7. Tavares TW, Bratko D, Blanch HW, Prausnitz JM (2004) Ion-specific effects in the colloid-colloid or protein-protein potential of mean force: Role of salt-macroion van der Waals interactions. *J Phys Chem B* 108(26):9228–9235.
8. Tavares TW, Bratko D, Prausnitz JM (2004) The role of salt-macroion van der Waals interactions in the colloid-colloid potential of mean force. *Curr Opin Colloid In* 9(1-2):81–86.
9. Lomakin A, Asherie N, Benedek GB (1999) Aeolotopic interactions of globular proteins. *Proc Natl Acad Sci USA* 96(17):9465–9468.
10. Lomakin A, Asherie N, Benedek GB (1996) Monte Carlo study of phase separation in aqueous protein solutions. *J Chem Phys* 104:1646–1656.
11. Carlsson F, Malmsten M, Linse P (2001) Monte Carlo simulations of lysozyme self-association in aqueous solution. *J Phys Chem B* 105:12189–12195.
12. Rosch TW, Errington JR (2007) Investigation of the phase behavior of an embedded charge protein model through molecular simulation. *J Phys Chem B* 111(43): 12591–12598.
13. Abramo MC, et al. (2012) Effective interactions in lysozyme aqueous solutions: A small-angle neutron scattering and computer simulation study. *J Chem Phys* 136(3): 035103.
14. Bianchi E, Largo J, Tartaglia P, Zaccarelli E, Sciortino F (2006) Phase diagram of patchy colloids: Towards empty liquids. *Phys Rev Lett* 97(16):168301.
15. Liu H, Kumar SK, Sciortino F (2007) Vapor-liquid coexistence of patchy models: Relevance to protein phase behavior. *J Chem Phys* 127(8):084902.
16. Gögelein C, et al. (2008) A simple patchy colloid model for the phase behavior of lysozyme dispersions. *J Chem Phys* 129(8):085102.
17. Acharya H, Vembanur S, Jamadagni SN, Garde S (2010) Mapping hydrophobicity at the nanoscale: Applications to heterogeneous surfaces and proteins. *Faraday Discuss* 146:353–365, discussion 367–393, 395–401.
18. Sear R (1999) Phase behaviour of a simple model of globular proteins. *J Chem Phys* 111(10):4800–4806.
19. Rosenbaum D, Zamora PC, Zukoski CF (1996) Phase behavior of small attractive colloidal particles. *Phys Rev Lett* 76(1):150–153.
20. Muschol M, Rosenberger F (1997) Liquid-liquid phase separation in supersaturated lysozyme solutions and associated precipitate formation/crystallization. *J Chem Phys* 107(6):1953–1962.
21. ten Wolde PR, Frenkel D (1997) Enhancement of protein crystal nucleation by critical density fluctuations. *Science* 277(5334):1975–1978.
22. Tavares TW, Prausnitz JM (2004) Analytic calculation of phase diagrams for solutions containing colloids or globular proteins. *Colloid Polym Sci* 282(6):620–632.
23. Sarangapani PS, Hudson SD, Jones RL, Douglas JF, Pathak JA (2015) Critical examination of the colloidal particle model of globular proteins. *Biophys J* 108(3):724–737.
24. Prausnitz J (2015) The fallacy of misplaced concreteness. *Biophys J* 108(3):453–454.
25. Taratuta VG, Holschbach A, Thurston GM, Blankschtein D, Benedek GB (1990) Liquid-liquid phase separation of aqueous lysozyme solutions: Effects of pH and salt identity. *J Phys Chem* 94(5):2140–2144.
26. Broide ML, Berland CR, Pande J, Ogun OO, Benedek GB (1991) Binary-liquid phase separation of lens protein solutions. *Proc Natl Acad Sci USA* 88(13):5660–5664.
27. Bončina M, Reščič J, Vlachy V (2008) Solubility of lysozyme in polyethylene glycol-electrolyte mixtures: The depletion interaction and ion-specific effects. *Biophys J* 95(3):1285–1294.
28. Rosenbaum DF, Kulkarni A, Ramakrishnan S, Zukoski CF (1999) Protein interactions and phase behavior: Sensitivity to the form of the pair potential. *J Chem Phys* 111(21): 9882–9890.
29. Moon YU, Anderson CO, Blanch HW, Prausnitz JM (2000) Osmotic pressures and second virial coefficients for aqueous saline solutions of lysozyme. *Fluid Phase Equilib* 168(2):229–239.
30. Nezbeda I (2003) Modeling of aqueous electrolytes at the molecular level: On the origin of the structure breaking and structure enhancement phenomena. *J Mol Liq* 103–104:309–317.
31. Bizjak A, Urbic T, Vlachy V, Dill KA (2009) Theory for the three-dimensional Mercedes-Benz model of water. *J Chem Phys* 131(19):194504.
32. Wertheim MS (1986) Fluids with highly directional attractive forces. III. Multiple attraction sites. *J Stat Phys* 42(3-4):459–476.
33. Wertheim MS (1986) Fluids with highly directional attractive forces. IV. Equilibrium polymerization. *J Stat Phys* 42(3-4):477–492.
34. Wertheim MS (1986) Fluids of dimerizing hard spheres, and fluid mixtures of hard spheres and dispheres. *J Chem Phys* 85(5):2929–2936.
35. Chapman WG, Jackson G, Gubbins K (1988) Phase equilibria of associating fluids chain molecules with multiple bonding sites. *Mol Phys* 65(5):1057–1079.
36. Hansen JP, McDonald IR (2006) *Theory of Simple Liquids* (Elsevier, Amsterdam).
37. Bonneté F, Vivarès D (2002) Interest of the normalized second virial coefficient and interaction potentials for crystallizing large macromolecules. *Acta Crystallogr D Biol Crystallogr* 58(Pt 10 Pt 1):1571–1575.
38. Chaplin MF (2001) Water: Its importance to life. *Biochem Mol Biol Educ* 29(2):54–59.
39. Grigsby JJ, Blanch HW, Prausnitz JM (2001) Cloud-point temperatures for lysozyme in electrolyte solutions: effect of salt type, salt concentration and pH. *Biophys Chem* 91(3):231–243.
40. Zhang Y, Cremer PS (2009) The inverse and direct Hofmeister series for lysozyme. *Proc Natl Acad Sci USA* 106(36):15249–15253.
41. Seručnik M, Bončina M, Lukšič M, Vlachy V (2012) Specific ion effects revealed in enthalpy of mixing of 3,3– and 6,6–ionenes with low molecular weight salts. *Phys Chem Chem Phys* 14(19):6805–6811.
42. Čebašek S, Seručnik M, Vlachy V (2013) Presence of hydrophobic groups may modify the specific ion effect in aqueous polyelectrolyte solutions. *J Phys Chem B* 117(13): 3682–3688.
43. Marcus Y (1997) *Ion Properties* (Dekker, New York).
44. George A, Wilson WW (1994) Predicting protein crystallization from a dilute solution property. *Acta Crystallogr D Biol Crystallogr* 50(Pt 4):361–365.
45. Haas C, Drenth J, Wilson WW (1999) Relation between the solubility of proteins in aqueous solutions and the second virial coefficient of the solution. *J Phys Chem B* 103(14):2808–2811.
46. Bonneté F, Finet S, Tardieu A (1999) Second virial coefficient: Variations with crystallization conditions. *J Cryst Growth* 196(2-4):403–414.
47. Neal BL, Asthagiri D, Velev OD, Lenhoff AM, Kaler EW (1999) Why is the osmotic second virial coefficient related to protein crystallization? *J Cryst Growth* 196(2-4): 377–387.
48. Ruppert S, Sandler SI, Lenhoff AM (2001) Correlation between the osmotic second virial coefficient and the solubility of proteins. *Biotechnol Prog* 17(1):182–187.
49. Valente JJ, Payne RW, Manning MC, Wilson WW, Henry CS (2005) Colloidal behavior of proteins: Effects of the second virial coefficient on solubility, crystallization and aggregation of proteins in aqueous solution. *Curr Pharm Biotechnol* 6(6):427–436.
50. Curtis RA, Prausnitz JM, Blanch HW, Blanch HW (1998) Protein-protein and protein-salt interactions in aqueous protein solutions containing concentrated electrolytes. *Biotechnol Bioeng* 57(1):11–21.
51. Haynes CA, Tamura K, Korfer HR, Blanch HW, Prausnitz JM (1992) Thermodynamic properties of aqueous α-chymotrypsin solutions from membrane osmometry measurements. *J Phys Chem* 96(2):905–912.
52. Tessier PM, et al. (2003) Predictive crystallization of ribonuclease A via rapid screening of osmotic second virial coefficients. *Proteins* 50(2):303–311.
53. Finet S, Skouri-Panet F, Casselyn M, Bonneté F, Tardieu A (2004) The Hofmeister effect as seen by SAXS in protein solutions. *Curr Opin Colloid Interface Sci* 9(1-2):112–116.